

1 **The new CLOCIT irradiation facility for $^{40}\text{Ar}/^{39}\text{Ar}$ geochronology: Characterization, comparison with**
2 **CLICIT, and implications for high-precision geochronology**

3 Daniel Rutte^{a,b}, Tim A. Becker^a, Alan L. Deino^a, Steven R. Reese^c, Paul R. Renne^{a,b}, and Robert A.
4 Schickler^c

5 ^a Berkeley Geochronology Center, 2455 Ridge Road, Berkeley, CA 94709, USA

6 ^b Department of Earth and Planetary Science, University of California, Berkeley, CA 94720, USA

7 ^c Nuclear Science and Engineering, Oregon State University, Corvallis, OR 97331, USA

8

9 **Abstract**

10 The Cadmium-Lined Outer-Core Irradiation Tube (CLOCIT) is a new irradiation facility for $^{40}\text{Ar}/^{39}\text{Ar}$
11 geochronology at the Oregon State University TRIGA[®] reactor. We report fluence (i.e., time-
12 integrated flux) parameters from the first four CLOCIT irradiations and compare them to the existing
13 Cadmium-Lined Inner-Core Irradiation Tube (CLICIT). CLOCIT provides an average neutron flux
14 equivalent of $1.45\text{--}1.53 \times 10^{-4} \text{ J/h}$; about 55 % of CLICIT. Radial fluence gradients are on the order of
15 $0.2\text{--}4.2 \text{ \%/cm}$. A planar fit of J -values results in residuals in the range of uncertainty in the J -value,
16 but systematic deviations resolve a non-planar component of the neutron flux field, which has also
17 been observed in CLICIT. Axial neutron fluence gradients are $0.6\text{--}1 \text{ \%/cm}$, compared to $0.7\text{--}1.6 \text{ \%/cm}$
18 for the CLICIT. Production rate ratios of interfering reactions are $(^{40}\text{Ar}/^{39}\text{Ar})_{\text{K}} = (4 \pm 6) \times 10^{-4}$ and
19 $(^{38}\text{Ar}/^{39}\text{Ar})_{\text{K}} = (1.208 \pm 0.002) \times 10^{-2}$, $(^{36}\text{Ar}/^{37}\text{Ar})_{\text{Ca}} = (2.649 \pm 0.014) \times 10^{-4}$, $(^{38}\text{Ar}/^{37}\text{Ar})_{\text{Ca}} = (3.33 \pm 0.12) \times 10^{-5}$,
20 and $(^{39}\text{Ar}/^{37}\text{Ar})_{\text{Ca}} = (9.1 \pm 0.28) \times 10^{-4}$, similar to the CLICIT values.

21

22 **Introduction**

23 The Cadmium-Lined Inner-Core Irradiation Tube (CLICIT) in the TRIGA[®] reactor at Oregon State
24 University (OSU) is a highly utilized irradiation facility for ⁴⁰Ar/³⁹Ar geochronology. In 2017, 79
25 irradiations were conducted for 23 labs from 12 different countries. Increased CLICIT demand has led
26 to sample backlogs of up to 300 h with OSU limited to 35 h of operation a week. Responding to
27 demand, a second facility, the Cadmium-Lined Outer-Core Irradiation Tube (CLOCIT), has been
28 commissioned. Here we report results from the first four irradiations spanning 17 minutes to 32.25
29 hours to characterize the new facility. We document average ³⁹Ar_k production rates, neutron fluence
30 gradients, and production rate ratios of interference reactions on Ca and K. We compare these values
31 to data from four recent CLICIT irradiations and production rate ratios on Ca and K established over
32 the long term.

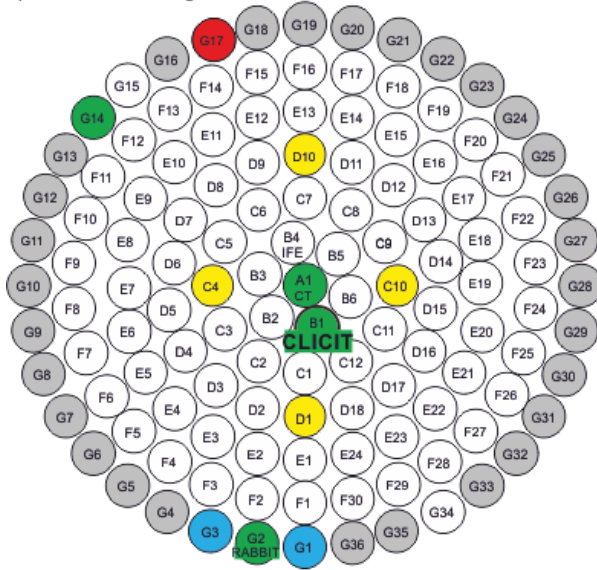
33

34 **Technical Specifications**

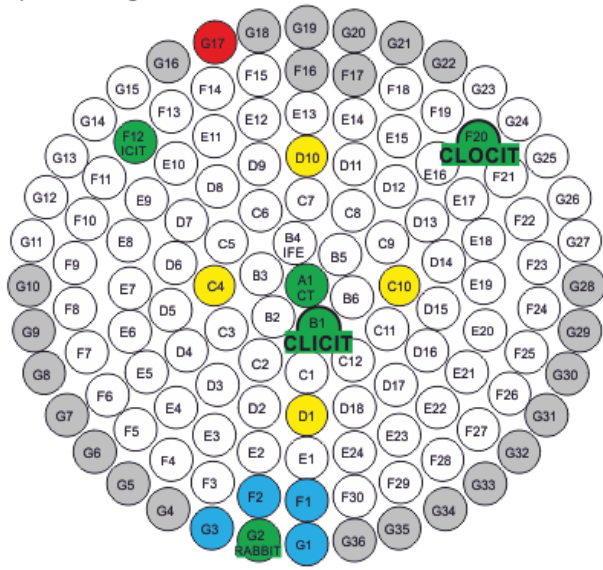
35 The CLOCIT is identical in construction to the CLICIT (Schickler et al., 2013). It consists of two
36 aluminium tubes: the inner tube has an outer diameter (OD) of 31.75 mm with a wall thickness of
37 1.47 mm. Surrounding the bottom of the inner tube is an outer tube which is 37.5 mm OD with a wall
38 thickness of 1.45 mm. This outer tube is 1067 mm long and serves as the facility's in-core terminus.
39 To minimize thermal neutron penetration into the irradiation facility, a 0.508 mm thick Cadmium
40 sleeve is wrapped around the outside of the inner aluminium tube and a disc of Cadmium is placed at
41 its bottom (Schickler et al., 2013). The facility allows irradiation of cylindrical packages with an OD of
42 22.86 mm and a height of 101.6 mm. The radial orientation is currently uncontrollable.

43 An Monte Carlo n-particle (MCNP) transport model of the reactor was employed to identify a
44 position for CLOCIT that provides a high fast-neutron flux at an acceptable loss of reactivity with the
45 cadmium sleeve introduced (Schickler and Reese, 2017). Position F20 near the core periphery, but
46 still surrounded by fuel elements provides this compromise (Figure 1). Two new fuel rods were added
47 to the core inventory and graphite rods were shuffled to minimize the loss in reactivity.

a) 2008-2017 configuration



b) new configuration



10 cm



48

49 **Figure 1.** Diagram of the reactor core configurations a) before and b) after installation of the CLOCIT.

50 The axial flux profiles in the CLOCIT and CLICIT were determined by activation of 55 cm long Al-Au

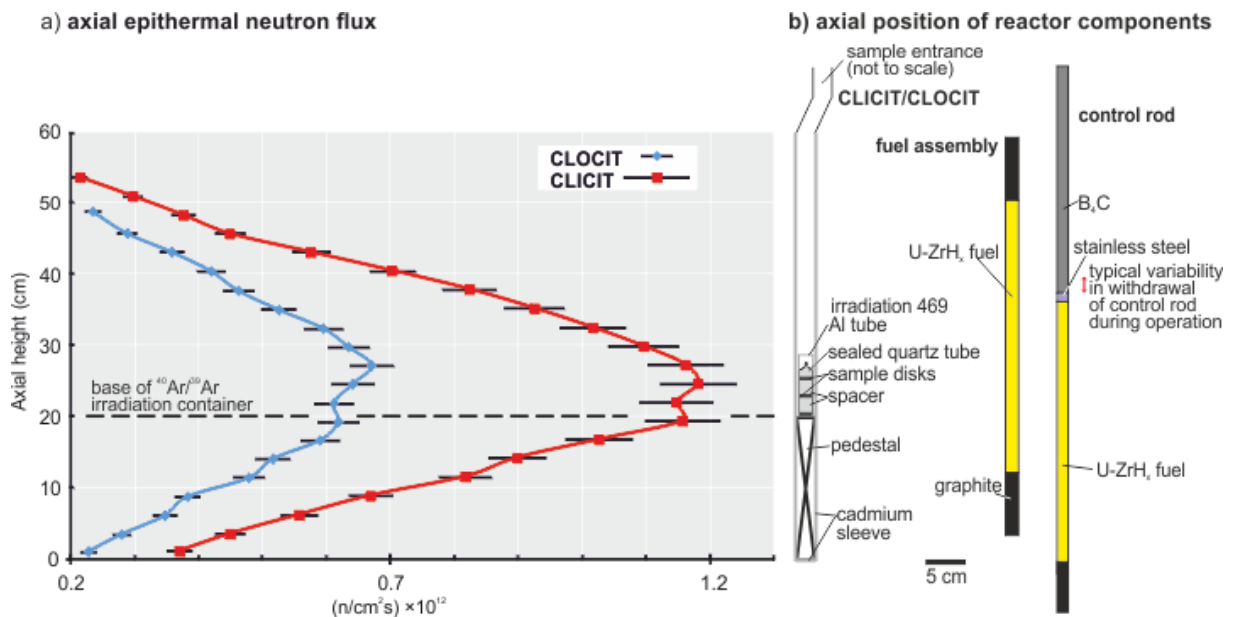
51 wire ($^{197}\text{Au}(n,\gamma)^{198}\text{Au}$) in a 2 min irradiation and subsequent gamma spectrometry of ^{198}Au activity.

52 The axial flux profile is the expected bell shape (Figure 2). OSU has historically determined 20 cm

53 above the base of the core as the desired location for irradiation of $^{40}\text{Ar}/^{39}\text{Ar}$ samples; thus a 20 cm

54 tall installed pedestal (“saddle”) ensures the samples are irradiated at the axial peak of the neutron

55 flux. The height can be adjusted to the needs of a specific irradiation by addition of sample spacers.



56

57 **Figure 2. a)** Axial flux profile of the CLOCIT and CLICIT determined by 2 min irradiation and
 58 subsequent γ -spectrometry of Al-Au wire. The dip at ~ 22 cm axial height is likely related to operation
 59 of the control rods at this height during startup. The dip is expected to disappear in longer irradiation
 60 times. b) Simplified geometry and relative axial position of the relevant components of the reactor in
 61 respect to the flux profile.

62

63 Methodology

64 We determined neutron fluences by irradiation and analysis of widely used geological sanidine
 65 standards from the Fish Canyon Tuff (FCs; ~ 28.2 Ma) and the Alder Creek rhyolite (ACs; ~ 1.18 Ma),
 66 and calculation of J -values (Formula 1; Grasty and Mitchell, 1966). Formula 1 shows the relation of
 67 the ratio of $^{40}\text{Ar}^*$ (radiogenic ^{40}Ar) and $^{39}\text{Ar}_K$ (^{39}Ar activated from K) in a standard of known age t with
 68 the neutron fluence Φ and their abstraction as the J -value. ^{39}K and ^{40}K are the respective natural
 69 abundances, λ is the total decay constant of ^{40}K , λ_e its electron capture decay constant, and σ the
 70 cross section of $^{39}\text{K}(n,p)^{39}\text{Ar}$ as a function of neutron energy E . For a detailed derivation see Grasty
 71 and Mitchell (1966).

$$J = \frac{{}^{39}\text{K}}{{}^{40}\text{K}} \frac{\lambda}{\lambda_e} \int \Phi(E)\sigma(E) dE = \frac{e^{\lambda t} - 1}{\frac{{}^{40}\text{Ar}^*}{{}^{39}\text{Ar}_K}} \quad \text{Formula 1}$$

73 Samples were irradiated in wells of variable geometry drilled in aluminium disks 18.54 mm OD. 4 to
 74 6 wells outlining a square, pentagon or hexagon along the edge of the disk - spanning about 15 mm
 75 across – and in some disks additional wells in the centre of the disk were loaded with 0.25–0.3 mm
 76 grains of FCs or 0.60-0.71 mm ACs. In irradiation 468 we included crushed synthetic Fe-doped (0.8
 77 wt.-%) aluminosilicate glass with about 11.3 wt.-% K and a grain size of 0.4–0.6 mm around the
 78 centre of level A and crushed natural fluorite with a grain size of 0.2–0.4 mm around the centre of
 79 level B. The disks were wrapped in Al foil, stacked and encapsulated in tight-fit glass tubing
 80 (preventing tilting of the disks), which in turn was encapsulated in an aluminium tube (Figure 2b).

81 We individually analyzed 5–10 grains of ACs and FCs per well, heated in one or two steps and
 82 calculated an inverse-variance weighted mean (in the following “weighted mean”) *J*-value for the
 83 respective well. All three Ar analysis lines at BGC (NEXUS, MAP1, and Noblesse) were involved, using
 84 measurement routines described in Niespolo et al. (2017). Typical uncertainties of *J*-values of
 85 individual wells are ~0.15–0.4 %. We determined a planar fit through the 4–8 wells of given *J*-value
 86 and calculated the deviation of each well from the fitted plane; the calculation considers uncertainty
 87 in *J*-value and predicts a *J*-value and respective uncertainty for any position. For *J*-value calculations
 88 we used ages of 28.201Ma (Kuiper et al., 2008) and 1.1848 Ma (Niespolo et al., 2017)) for FCs and
 89 ACs, respectively. Other ages are in use for these standards but the values used are irrelevant for the
 90 present purposes so long as they are internally consistent as was demonstrated by Niespolo et al.
 91 (2017).

92 **Results and Discussion**

93 **Average Neutron Flux**

94 The average flux in the CLOCIT irradiations is equivalent to $1.45\text{--}1.53 \times 10^{-4} \text{ J/h}$ (Table 1). These values
 95 compare to $2.62\text{--}2.72 \times 10^{-4} \text{ J/h}$ of the last four CLICIT irradiations analyzed at BGC. Thus to achieve a
 96 similar J -value, CLOCIT irradiations should be about 1.8 times longer than those in the CLICIT.

97 Table 1. Comparison of fluence parameters of four irradiations in CLOCIT and CLICIT, respectively.

98

Irradiation	duration [h]	level	n	height in irradiation container [cm]	radial gradient [%/cm]	ave. unc. of J-values [%]	max. dev. from planar fit [%]	axial gradient [%/cm]	J/h $\times 10^{-4}$
CLICIT									
468	32.25	C	4	5.3	0.87	0.18	0.01		1.53
	32.25	B	4	2.8	0.51	0.17	0.13	1.0	1.51
	32.25	A	4	0.2	0.20	0.17	0.03		1.45
470	0.28	A	4	0.2	1.15	0.23	0.26	NA	1.51
471	0.83	A	4	1.9	3.69	0.18	0.06		1.47
	0.83	B	4	1.3	4.10	0.18	0.35	0.3	1.47
	0.83	C	4	0.8	4.01	0.19	0.12		1.47
	0.83	D	5	0.2	4.24	0.24	0.15		1.46
472	5	A	4	1.9	2.17	0.10	0.01		1.47
	5	B	4	1.3	1.93	0.12	0.07	0.6	1.47
	5	C	4	0.0	1.91	0.17	0.13		1.46
	5	D	4	0.2	2.29	0.13	0.05		1.46
CLOCIT									
464	0.5	A	4	1.0	0.47	0.40	0.02	1.6	2.72
	0.5	B	4	0.2	1.23	0.30	0.25		2.68
465	2	A	4	1.0	1.07	0.41	0.31	1.4	2.65
	2	B	4	0.2	0.67	0.21	0.20		2.62
466	20	4	6	2.9	0.31	0.31	0.33	0.7	2.70

	20	3	6	2.0	0.36	0.25	0.39		2.69
	20	2	6	1.1	0.29	0.25	0.41		2.68
	20	1	6	0.2	0.45	0.32	0.30		2.65
467	1	A	6	2.9	0.07	0.49	0.22		2.70
	1	B	6	2.0	0.22	0.37	0.68	0.9	2.68
	1	C	6	1.1	0.53	0.49	0.14		2.65
	1	D	3	0.2	0.88	0.71	NA		2.64

99

100

101 Fluence Gradients

102 The axial fluence increases upwards from the basal standard irradiation position by an average of
 103 about 0.6–1 %/cm in the CLOCIT, similarly the CLICIT (0.7–1.6 %/cm; Table 1). For irradiation sample
 104 holders utilizing wells in an aluminium disk, these gradients may be significant when standards and
 105 unknowns have different fill levels in the wells.

106 We calculated radial gradients based on planar fit through the weighted mean *J*-values of wells. The
 107 maximum deviation of individual wells from the planar fit is typically below 0.3 % for both CLICIT and
 108 CLOCIT and in the range of analytical uncertainty of the *J*-value indicating that planar fits provide a
 109 decent approximation on the scale of a disk (Table 1). However, we found a systematic deviation of
 110 the central wells to lower *J*-values. The 7 disks with standards in the central well (both CLICIT and
 111 CLOCIT irradiations) gave a weighted mean analyzed-over-predicted ratio of 0.9982 ± 0.0009
 112 (MSWD=0.73), i.e., in average 0.2 % lower values. Both the larger distance of the central well to the
 113 surrounding fuel elements and neutron shielding by the irradiation container and samples may
 114 contribute to this. Rutte et al. (2015) provides a simulated neutron flux distribution that illustrates
 115 the significantly non-planar axial variation over the irradiation channel in a comparable research
 116 reactor without an irradiation target introduced (their figure 4b). Shielding includes consumption of
 117 neutrons by capture and transfer reactions as well as neutron moderation by scattering; moderation

118 lowers the probability of $^{39}\text{K}(n,p)^{39}\text{Ar}$ to occur due to the smaller cross-section for lower energy
119 neutrons.

120 These data agree with long term observations at the Berkeley Geochronology Center; in practice this
121 has led to either completely avoiding extrapolating J -values determined from, e.g., outer ring
122 standards to inner ring samples (Figure 3) or case to case assessment of the effects and mitigation by
123 e.g. bracketing. The following values are calculated excluding the central well as a constraint for the
124 planar fit.

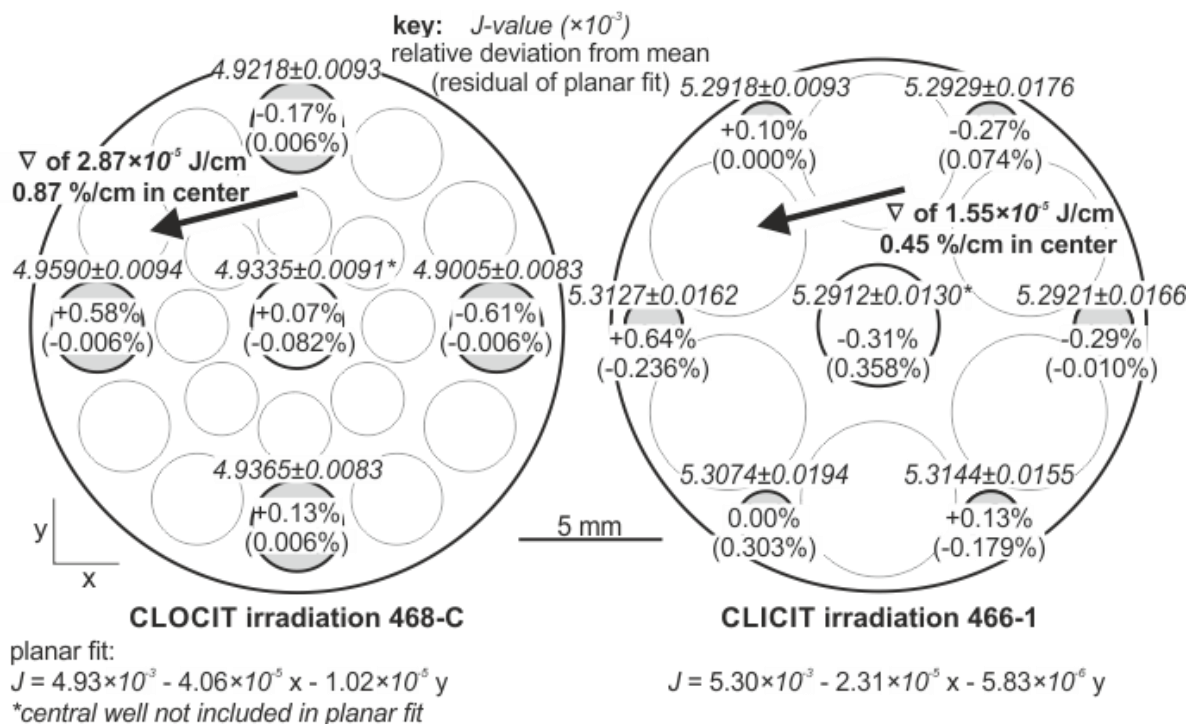
125 The planar fits (through the outer ring) provide a gradient in the form of J/cm ; to allow comparison
126 we converted it to $\%/ \text{cm}$ for the respective centre of each disk (Figure 3, Table 1). In the four CLOCIT
127 irradiations, radial gradients range 0.2–4.2 $\%/ \text{cm}$, i.e., up to $\sim 6\%$ variability across a single disk
128 (Table1). These compare to radial gradients in the CLICIT of up to 1.2 $\%/ \text{cm}$ (Table1). Figure 3 shows
129 an example of radial gradients observed in two disks irradiated in CLICIT and CLOCIT. Some
130 irradiations display a trend with axially upward increasing radial gradients (e.g., CLOCIT irradiation
131 468) or axially upward decreasing radial gradients (e.g., CLICIT irradiation 467; Table 1); in both
132 irradiations fluence increases axially upwards. In CLOCIT and CLICIT the radial gradients vary more in
133 between irradiations than in between disks of an individual irradiation (Table 1). While higher radial
134 gradients in CLOCIT compared to CLICIT are readily explained by the fact that it has less fuel on one
135 side, the variability of determined axial fluence gradients between irradiations – in both facilities – is
136 currently unknown.

137 Which factors may cause variability of the fluence field in between irradiations? (i) The startup of the
138 reactor to full power takes about 3 minutes and several more minutes until stable operation -
139 including secular equilibration of delayed neutron precursors - is reached; the exact timing is not well
140 known. Higher flux gradients have to be expected for this phase. In shorter irradiations, initially
141 higher flux gradients exert greater influence on the resulting fluence gradient. This may explain the
142 highest fluence gradients for the 50 min irradiation 471 and the smallest fluence gradients in the

143 32.25 h irradiation 468. However, the 16.8 min irradiation 470 with intermediate gradients suggests
144 this cannot be the only factor. (ii) Over each day and the course of a week of operation the
145 concentration of the neutron absorber ^{135}Xe ($T_{1/2} = 9.2\text{h}$) increases (“Xenon poisoning”) in the fuel
146 elements and the resulting loss in criticality requires further withdrawal of the control rods. Over the
147 course of a week this may result in about 2.5 cm difference in the insertion depth of the control rods
148 (Figure 2b). It is unclear how this variation changes the flux field in at the sample position. (iii)
149 Contemporaneous with $^{40}\text{Ar}/^{39}\text{Ar}$ sample irradiation in CLOCIT, the other facilities (CLICIT, ICIT; Figure
150 1) are loaded with different materials that may influence the flux field in the reactor. Irradiations 471
151 and 472 for which we determined factor 2 different fluence gradients were irradiated in the same
152 day, with the same irradiations continuing in CLICIT and ICIT suggesting this factor cannot explain
153 their variability. 471 was irradiated in the afternoon with the control rods being 0.8 cm more
154 withdrawn compared to 472 in the morning.

155 For the irradiation employed herein on aluminium disks we found 4 standards on the outer ring to be
156 sufficient to predict J-values on that outer ring in CLICIT. Depending on the scope of the study a
157 higher density may be advisable for CLOCIT. For studies requiring highest precision such as standard
158 intercalibration CLICIT should - with current knowledge - be preferred over CLOCIT. Given the larger
159 gradients in CLOCIT, the size of wells in disks should be limited, e.g., individual crystals in a well with
160 5 mm diameter may experience 2 % different fluence resulting in overdispersion of single crystal
161 ages. While the planar fit can provide satisfactory accuracy for most applications, the highest
162 precision can be achieved by mixing standards and unknowns in a single well given a sufficient age
163 difference and single grain analysis to enable distinction between standards and unknowns after the
164 irradiation. With very similar axial gradients compared to CLICIT, CLOCIT provides the same qualities
165 for stacked irradiations where samples and unknowns are arranged in line.

166



167

168 **Figure 3.** Maps of 21 and 13-well aluminium irradiation disks. Highlighted wells include standards.

169 Weighted mean J -value, deviation from disk mean, and residual of planar fit are indicated. Arrows

170 trace the gradient (∇); the similar orientation is coincident. Uncertainties here and throughout are

171 given at the 1σ level. Point of origin is in the disk centres.

172 **Interference Reactions**

173 **^{40}Ar and ^{39}Ar from K**

174 We determined the production ratios of $(^{40}\text{Ar}/^{39}\text{Ar})_{\text{K}}$ and $(^{38}\text{Ar}/^{39}\text{Ar})_{\text{K}}$ which are produced via

175 $^{39}\text{K}(n,p)^{39}\text{Ar}$, $^{40}\text{K}(n,p)^{40}\text{Ar}$, $^{39}\text{K}(n,d)^{38}\text{Ar}$, and $^{41}\text{K}(n,\alpha\beta)^{38}\text{Ar}$ reactions. We analyzed CLOCIT irradiated

176 kalsilite by single-step-fusion of 3-8 grains. 23 aliquots yielded a weighted mean of $(4\pm 6) \times 10^{-4}$ for

177 $(^{40}\text{Ar}/^{39}\text{Ar})_{\text{K}}$ and $(1.208\pm 0.002) \times 10^{-2}$ for $(^{38}\text{Ar}/^{39}\text{Ar})_{\text{K}}$ (Figure 4). These values are indistinguishable from

178 $(7.3\pm 0.9) \times 10^{-4}$ and $(1.196\pm 0.013) \times 10^{-2}$ for CLICIT (Renne et al., 2005). Long term repetition of this

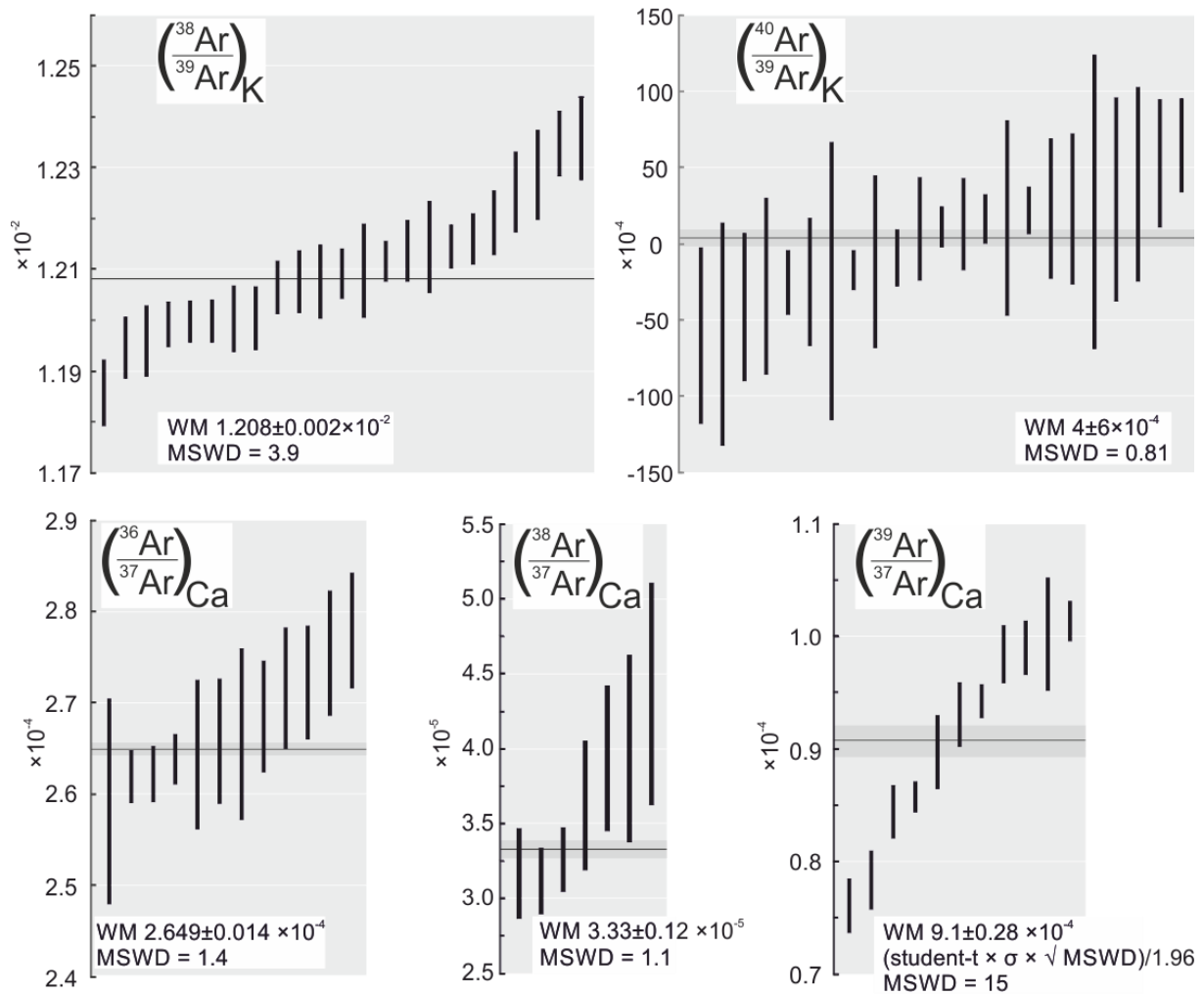
179 experiment is required to reduce uncertainty of the determined value for $(^{40}\text{Ar}/^{39}\text{Ar})_{\text{K}}$ which is

180 challenging to analyze precisely due to the low $^{40}\text{Ar}_{\text{K}}$ production rate in Cd-shielded irradiations.

181 **^{36}Ar , ^{37}Ar , ^{38}Ar , and ^{39}Ar from Ca**

182 We determined the production ratios of $(^{36}\text{Ar}/^{37}\text{Ar})_{\text{Ca}}$, $(^{38}\text{Ar}/^{37}\text{Ar})_{\text{Ca}}$ and $(^{39}\text{Ar}/^{37}\text{Ar})_{\text{Ca}}$ which are mainly
183 produced via $^{40}\text{Ca}(n,\alpha)^{36}\text{Ar}$, $^{40}\text{Ca}(n,\alpha)^{37}\text{Ar}$, $^{42}\text{Ca}(n,\alpha)^{38}\text{Ar}$, $^{43}\text{Ca}(n,\alpha)^{39}\text{Ar}$, $^{42}\text{Ca}(n,\alpha)^{39}\text{Ar}$, and
184 $^{43}\text{Ca}(n,\alpha)^{39}\text{Ar}$. We analyzed fluorite irradiated in CLOCIT by single-step-fusion with a CO_2 laser.
185 Fluorite is semitransparent to the $\sim 10\ \mu\text{m}$ wavelength of the laser so it was co-loaded with previously
186 degassed and crushed basalt glass which co-fused the fluorite when heated. 11 aliquots of 5 to 15
187 grains each were analyzed. In contrast to the other isotopes, ^{39}Ar signals were only 10-30 times
188 above background for most of the aliquots. The rise rates of the ^{39}Ar beam were significantly larger
189 than those of the background measurements due to memory effects in the mass spectrometer. The
190 calculated $^{39}\text{Ar}/^{37}\text{Ar}$ are overdispersed with an MSWD of 15, likely an effect of the low signal intensity
191 and high rise rate; both effects are poorly quantified by the common uncertainty determination from
192 intercept extrapolation. To give a more realistic representation of the uncertainty of the weighted
193 mean of $(^{39}\text{Ar}/^{37}\text{Ar})_{\text{Ca}}$ we multiplied the sigma uncertainty with the square-root of the MSWD and
194 Students-t for N-1 degrees of freedom; see Ludwig (2012) for details.

195
196 The resulting weighted mean values are $(^{36}\text{Ar}/^{37}\text{Ar})_{\text{Ca}} = (2.649 \pm 0.014) \times 10^{-4}$, $(^{38}\text{Ar}/^{37}\text{Ar})_{\text{Ca}} = (3.33 \pm 0.12)$
197 $\times 10^{-5}$ and $(^{39}\text{Ar}/^{37}\text{Ar})_{\text{Ca}} = (9.1 \pm 0.28) \times 10^{-4}$. These compare to $(^{36}\text{Ar}/^{37}\text{Ar})_{\text{Ca}} = (2.702 \pm 0.004) \times 10^{-4}$,
198 $(^{38}\text{Ar}/^{37}\text{Ar})_{\text{Ca}} = (1.96 \pm 0.08) \times 10^{-5}$ and $(^{37}\text{Ar}/^{39}\text{Ar})_{\text{Ca}} = (7.02 \pm 0.12) \times 10^{-4}$ in CLICIT (Renne et al., 2015).



199

200 **Figure 4.** Ratios of Ar isotope production rates from K and Ca in CLOCIT determined from irradiated
 201 K-rich glass and fluorite (CaF₂).

202 **Conclusions**

203 The average neutron flux is about 1.8 times lower in CLOCIT compared to CLICIT. Production rate
 204 ratios of Ar isotopes from Ca and K are similar. We find up to 3 times higher radial fluence gradients
 205 and similar axial fluence gradients. Planar fitting of *J*-values on an irradiation disk results in residuals
 206 on the order of uncertainty in *J*, but systematic deviations can be recognized. At the current state of
 207 the technique, the non-planar component of the reactors neutron flux field becomes resolvable and
 208 needs to be accounted for to reach even higher precision and aspiring to the 0.1 % goal defined by
 209 the EARTHTIME community.

210

211 **Acknowledgements**

212 We thank two anonymous reviewers and editor Jacinta Enzweiler for handling the manuscript. D.R.
213 was supported by DFG research scholarship RU 2065/1-1. Instrumentation was funded by NSF grants
214 EAR-9005260, 1322017 and SBR-9601592. Facilities support from the Ann and Gordon Getty
215 Foundation is gratefully acknowledged.

216

217 **References**

- 218 Grasty R. L. and Mitchell J. G. (1966) Single sample potassium-argon ages using the omegatron. *Earth*
219 *Planet. Sci. Lett.* **1**, 121–122.
- 220 Kuiper K. F., Deino A., Hilgen F. J., Krijgsman W., Renne P. R. and Wijbrans J. R. (2008) Synchronizing
221 Rock Clocks of Earth History. *Science (80-.)*. **320**, 500–504. Available at:
222 <http://www.sciencemag.org/cgi/doi/10.1126/science.1154339>.
- 223 Ludwig K. R. (2012) User's Manual for Isoplot 3.75. *Berkeley Geochronol. Cent. Spec. Publ.* **5**.
- 224 Niespolo E. M. E. M., Rutte D., Deino A. L. A. L. and Renne P. R. P. R. (2017) Intercalibration and age of
225 the Alder Creek sanidine $^{40}\text{Ar}/^{39}\text{Ar}$ standard. *Quat. Geochronol.* **39**, 205–213. Available at:
226 <http://linkinghub.elsevier.com/retrieve/pii/S1871101416300589>.
- 227 Renne P. R., Knight K. B., Nomade S., Leung K.-N. and Lou T.-P. (2005) Application of deuterium–
228 deuterium (D–D) fusion neutrons to $^{40}\text{Ar}/^{39}\text{Ar}$ geochronology. *Appl. Radiat. Isot.* **62**, 25–32.
229 Available at: <http://linkinghub.elsevier.com/retrieve/pii/S0969804304003951>.
- 230 Renne P. R., Sprain C. J., Richards M. A., Self S., Vanderkluysen L. and Pande K. (2015) State shift in
231 Deccan volcanism at the Cretaceous–Paleogene boundary, possibly induced by impact. *Science*
232 *(80-.)*. **350**, 76 LP-78.
- 233 Rutte D., Pfänder J. A., Koleška M., Jonckheere R. and Unterricker S. (2015) Radial fast-neutron
234 fluence gradients during rotating $^{40}\text{Ar}/^{39}\text{Ar}$ sample irradiation recorded with metallic fluence
235 monitors and geological age standards. *Geochemistry, Geophys. Geosystems* **16**, 336–345.
236 Available at: <http://doi.wiley.com/10.1002/2014GC005611>.
- 237 Schickler R. A., Marcum W. R. and Reese S. R. (2013) Comparison of HEU and LEU neutron spectra in
238 irradiation facilities at the Oregon State TRIGA® Reactor. *Nucl. Eng. Des.* **262**, 340–349.
- 239 Schickler R. and Reese S. (2017) Installation of a Second CLICIT Irradiation Facility at the Oregon State
240 TRIGA Reactor. In *International Group on Research Reactors Conference Proceedings*

241